ISSN 1674-1056
http://cpb.iphy.ac.cn
http://iopscience.iop.org/cpb
中国物理 B
Chinese Physics
中国物理
Chinese Physics B

Charge-state populations for the neon-XFEL system

Ping Deng(邓萍), Gang Jiang(蒋刚)

Citation: Chin. Phys. B . 2019, 28(6): 063203. **doi:** 10.1088/1674-1056/28/6/063203
Journal homepage: http://cpb.iphy.ac.cn; http://iopscience.iop.org/cpb

What follows is a list of articles you may be interested in

Single and double Auger decay of 4f-ionized mercury including cascade and direct processes

Yu-Long Ma(马玉龙), Fu-Yang Zhou(周福阳), Zhen-Qi Liu(刘振旗), Yi-Zhi Qu(屈一至)

Chin. Phys. B . 2018, 27(6): 063201. **doi:** 10.1088/1674-1056/27/6/063201

Simulating resonance-mediated two-photon absorption enhancement in rare-earth ions by a rectangle phase modulation

Da-Long Qi(齐大龙), Ye Zheng(郑烨), Wen-Jing Cheng(程文静), Yun-Hua Yao(姚云华), Lian-Zhong Deng(邓联忠), Dong-Hai Feng(冯东海), Tian-Qing Jia(贾天卿), Zhen-Rong Sun(孙真荣), Shi-An Zhang(张诗按)

Chin. Phys. B . 2018, 27(1): 013202. **doi:** 10.1088/1674-1056/27/1/013202

Characterizing passive coherent population trapping resonance in cesium vapor cell filled with neon as buffer gas

Liu Zhi, Wang Jie-Ying, Diao Wen-Ting, He Jun, Wang Jun-Min

Chin. Phys. B . 2013, 22(4): 043201. **doi:** 10.1088/1674-1056/22/4/043201

Charge-state populations for the neon-XFEL system*

Ping Deng(邓萍)[1,2] and Gang Jiang(蒋刚)[1,2,†]

[1] Institute of Atomic and Molecular Physics, Sichuan University, Chengdu 610065, China
[2] Key Laboratory of High Energy Density Physics and Technology, Ministry of Education, Chengdu 610065, China

(Received 14 November 2018; revised manuscript received 3 April 2019; published online 8 May 2019)

The interaction between neon and x-ray free-electron lasers with different laser parameters is systematically studied by solving a set of coupled rate equations. As an example, the evolution of $1s^1 2s^2 2p^6$ configuration is given under different incident photon numbers, pulse widths, and photon energies. We have also determined all of the charge-state populations as a function of three laser pulse parameters by averaging over time. The result shows that the variations of these charge-state populations demonstrate a pattern when the pulse width is shorter than 10 fs: some of the charge-states decrease rapidly, while the others rise but remain relatively constant for pulse width larger than 10 fs. The variation of the average charge with three parameters has also obtained. The average charge decreases for a pulse width shorter than 10 fs but remains basically unchanged for a pulse width longer than 10 fs.

Keywords: x-ray free electron lasers, neon, charge-state population, pulse width

PACS: 32.80.Hd, 32.80.Aa **DOI:** 10.1088/1674-1056/28/6/063203

1. Introduction

X-ray free-electron lasers (XFEL) with high intensity coherent radiation pulses enable the exploration of structures and dynamical processes of atomic and molecular systems at the angstrom-femtosecond scale.[1] With advances in technology,[1–9] XFEL offers many possibilities that would have been inconceivable with conventional light sources.[10–12] Consequently, many important scientific achievements have been made in the fields of atomic, molecular, and optical physics,[2,13,14] condensed matter physics,[15] matter in extreme conditions,[16] chemistry and soft matters,[17] and biology,[18,19] *etc*. Novel phenomena appear when XFEL interact with atoms and ions,[20] such as saturation absorption,[21] x-ray transparency,[2,20,22] and hollow atoms.[2,23] In particular, the formation of hollow atoms following continuous photoionization of the inner shells leads to x-ray transparency.[2,20]

Both experimental[2] and theoretical[24] results have revealed how the electrons of a free neon atom response to ultra intense, ultrafast x-ray pulses. When XFEL interact with the neon atom, various ions are produced. These ions populations have been theoretically simulated.[25–27] In the hard x-ray region, the single-photon ionization dominates, and inner-shell electrons are photo-ejected preferentially when allowed. All inner-shell electrons for a given atom may be removed before Auger decay or other relaxation processes occur when inner-shell photoabsorption reaches saturation.[2,23,24] Furthermore, the inner-shell resonant absorption will play an important role in neon irradiated by x-ray pulses at a wide photon energy range of 850 eV–1350 eV.[28] However, both in theory and experiment, the variations of ion populations with laser parameters have not been given in detail. If we know these variations, then we can further understand the interaction mechanism of atoms with XFEL. This also provides references for parameter selections in the experiment involving XFEL. Consequently, we will explore the variation of the charge-state population of neon with different laser parameters in this work.

2. Theoretical method

In this work, the related atomic data are investigated by using the distorted wave approximation implemented in the Flexible Atomic Code(FAC).[29] The atomic structure calculation is based on the Dirac equation by diagonalizing the relativistic Hamiltonian

$$H = \sum_{i=1}^{N} H_{\mathrm{D}}(i) + \sum_{i<j}^{N} \frac{1}{r_{ij}}, \tag{1}$$

where $H_{\mathrm{D}}(i)$ is the single-electron Dirac Hamiltonian for the potential of the nuclear charge. The atomic basis states Φ_j are antisymmetric sums of the products of N one-electron Dirac spinors $\varphi_{n\kappa m}$,

$$\varphi_{n\kappa m} = \frac{1}{r}\begin{pmatrix} P_{n\kappa}(r)\chi_{\kappa m}(\theta,\psi,\sigma) \\ \mathrm{i}Q_{n\kappa}(r)\chi_{-\kappa m}(\theta,\psi,\sigma) \end{pmatrix}, \tag{2}$$

where $P_{n\kappa}(r)$ is the radial function of the large component, $Q_{n\kappa}(r)$ the radial function of the small component, and $\chi_{\kappa m}(\theta,\psi,\sigma)$ the spherical spinor. Here n is the principal quantum number, κ the angular-symmetry quantum number, and m the magnetic quantum number. So an approximate atomic state is given by a linear combination of basis states with the same symmetry,

$$\psi = \sum_j b_j \Phi_j, \tag{3}$$

*Project supported by the National Natural Science Foundation of China (Grant No. 11474208).
†Corresponding author. E-mail: gjiang@scu.edu.cn
© 2019 Chinese Physical Society and IOP Publishing Ltd

where b_j are the expansion coefficients.

2.1. Photoionization process

The partial photoionization cross section can be expressed by the differential oscillator strength,

$$\sigma_p = 2\pi\alpha\frac{\mathrm{d}f}{\mathrm{d}E}, \tag{4}$$

where α is the fine structure constant and $\mathrm{d}f/\mathrm{d}E$ is the differential oscillator strength calculated by

$$\frac{\mathrm{d}f}{\mathrm{d}E} = \frac{\omega}{g_\mathrm{i}}[L]^{-1}(\alpha\omega)^{2L-2}\sum_{\kappa J_\mathrm{T}}\left|\langle\psi_\mathrm{f},\kappa;J_\mathrm{T}\|O^L\|\psi_\mathrm{i}\rangle\right|^2, \tag{5}$$

where g_i is the statistical weight of the bound states before the photoionization takes place, and the photon energy is denoted by $E=\hbar\omega$. Here L is the rank of the multipole operator inducing the transition, $[L]$ denotes $2L+1$. And ψ_i is the wave function of the initial state, ψ_f the wave function of the final state, κ the angular-symmetry quantum number of the free electron, J_T the total angular momentum when the target state is coupled to the continuum orbital, and O^L the multiple operator inducing the transition.

2.2. Relaxation process

In the first-order perturbation theory, the single Auger decay rate can be expressed as,

$$R_\mathrm{a} = 2\sum_\kappa\left|\langle\psi_\mathrm{f},\kappa;J_\mathrm{T}M_\mathrm{T}|\sum_{i<j}\frac{1}{r_{ij}}|\psi_\mathrm{i}\rangle\right|^2, \tag{6}$$

where M_T is the projection of the total angular momentum, and κ the angular-symmetry quantum number of the free electron.

The fluorescence decay rate is calculated in the single multipole approximation. The line strength of the transition is

$$S_\mathrm{fi} = \left|\langle\psi_\mathrm{f}\|O^L_\mathrm{M}\|\psi_\mathrm{i}\rangle\right|^2, \tag{7}$$

where O^L_M is the multipole operator. The weighted oscillator strength and fluorescence decay rates are given by,

$$gf_\mathrm{fi} = [L]^{-1}\omega_\mathrm{fi}(\alpha\omega_\mathrm{fi})^{2L-2}S_\mathrm{fi}, \tag{8}$$

$$R_\mathrm{f} = 2\alpha^3\omega_\mathrm{fi}^2 gf_\mathrm{fi} = 2[L]^{-1}(\alpha\omega_\mathrm{fi})^{2L+1}\left|\langle\psi_\mathrm{f}\|O^L_\mathrm{M}\|\psi_\mathrm{i}\rangle\right|^2, \tag{9}$$

where $\omega_\mathrm{fi}=|E_\mathrm{f}-E_\mathrm{i}|$ is the transition energy.

2.3. Rate equations for photoionization and relaxation dynamics

To simulate the dynamic process of neon irradiated by intense x-ray pulses, we need to establish a set of coupled rate equations that have been successfully used to describe the transitions among all possible electron configurations,[2,24]

$$\frac{\mathrm{d}}{\mathrm{d}t}n_\alpha(t) = \sum_{\alpha'\neq\alpha}^{\text{all config}}[\Gamma_{\alpha'\to\alpha}n_{\alpha'}(t)-\Gamma_{\alpha\to\alpha'}n_\alpha(t)], \tag{10}$$

where $n_\alpha(t)$ is the fractional population evolution of the α-th configuration, and $\Gamma_{\alpha\to\alpha'}$ the rate coefficient for the transition from configuration α to α'. Here Γ may be the time-independent Auger rate R_a or fluorescence rate R_f, as well as the photoionization rate R_p given by $\sigma_p\times J(t)$, where $J(t)$ is the photon flux of the x-ray pulse. And $J(t)$ is given by the XFEL intensity,

$$J(t) = \frac{I(t)}{E}, \tag{11}$$

where $I(t)$ is the XFEL intensity which has a Gaussian profile on time in the present work. According to Refs. [25] and [26], $I(t)$ is expressed as follows:

$$I(t) = 2\sqrt{\frac{\ln 2}{\pi}}\frac{N_\mathrm{p}E}{SW}\exp\left[-4ln2\frac{(t-t_1)^2}{W^2}\right], \tag{12}$$

where S is the beam size, N_p the number of incident photons, W the Gaussian pulse width (FWHM), and t_1 the center of temporal profile. We utilize a fourth-order Runge–Kutta integrator to solve these coupled rate equations using these rates as input parameters. We include all of the possible photoionization and relaxation processes for each configuration.

When we study the effects of laser parameters achievable using XFEL[1,30] on neon, the Gaussian pulse width (FWHM) in our calculations varies from $W=1$ to 150 fs. The number N_p of incident photons is selected to be 10^9, 10^{10}, 10^{11}, and 10^{12} with beam size S of 100 nm×100 nm, corresponding to a fluence of 10^3, 10^4, 10^5, and 10^6 photons/Å^2, while the photon energy is chosen at $E=2$ keV, 4 keV, 6 keV, and 8 keV. Based on these selected photon energies, we can ignore the inner-shell resonant absorption.[28] In our simulation, we consider photoionization (P), Auger decay (A), and fluorescence decay (F). And photoionization cross sections σ_p of each shell for different configurations of neon at photon energies $E=4$ keV, 6 keV, and 8 keV calculated using FAC are shown in Table 1, while σ_p at $E=2$ keV, Auger decay rates R_a and fluorescence decay rates R_f of neon are taken from Refs. [20] and [31], which are also calculated by FAC. It can be seen that σ_p decrease with the increase of the selected photon energy. This is also expected based on the scaling behavior of the photoionization cross-section in the high-energy limit, $\sigma_\mathrm{p}\propto E^{-7/2}$ ($l=0$).[32] Based on these atomic data, the maximum and minimum of R_a, R_f, and σ_p for all configurations are obtained, as shown in Table 2 and 3. It can be seen from Table 2 that the orders of magnitude of R_a and R_f are 10^{13} s^{-1} $\sim 10^{15}$ s^{-1} and 10^8 s^{-1} $\sim 10^{13}$ s^{-1}. The orders of magnitude of σ_p are 10^{-22} cm^2 $\sim 10^{-20}$ cm^2, 10^{-23} cm^2 $\sim 10^{-20}$ cm^2, 10^{-24} cm^2 $\sim 10^{-21}$ cm^2, and 10^{-24} cm^2 $\sim 10^{-21}$cm^2 at $E=$ 2 keV, 4 keV, 6 keV, and 8 keV, respectively, see Table 3. For a given laser parameter, the order of magnitude of the photoionization rate R_p is equal to the order of magnitude of σ_p multiplied by $J(t)$.

Table 1. X-ray absorption cross sections σ_p (10^{-20} cm^2) for all configurations of neon at 4 keV, 6 keV, and 8 keV.

Ne	4 keV			6 keV			8 keV		
	1s	2s	2p	1s	2s	2p	1s	2s	2p
$1s^2 2s^2 2p^6$	0.5465	0.0269	0.0031	0.1651	0.0091	0.0007	0.0693	0.0045	0.0003
$1s^1 2s^2 2p^6$	0.3078	0.0325	0.0064	0.0916	0.0101	0.0013	0.0380	0.0042	0.0003
$1s^2 2s^1 2p^6$	0.5497	0.0143	0.0042	0.1664	0.0044	0.0009	0.0698	0.0019	0.0002
$1s^2 2s^2 2p^5$	0.5455	0.0285	0.0036	0.1652	0.0089	0.0008	0.0693	0.0037	0.0002
$1s^0 2s^2 2p^6$	–	0.0379	0.0081	–	0.0118	0.0016	–	0.0050	0.0005
$1s^1 2s^1 2p^6$	0.3108	0.0173	0.0072	0.0923	0.0054	0.0014	0.0382	0.0023	0.0004
$1s^1 2s^2 2p^5$	0.3072	0.0347	0.0061	0.0912	0.0109	0.0012	0.0378	0.0046	0.0004
$1s^2 2s^0 2p^6$	0.5561	–	0.0048	0.1677	–	0.0010	0.0701	–	0.0003
$1s^2 2s^1 2p^5$	0.5509	0.0153	0.0041	0.1663	0.0048	0.0008	0.0696	0.0020	0.0002
$1s^2 2s^2 2p^4$	0.5458	0.0306	0.0033	0.1649	0.0096	0.0007	0.0692	0.0041	0.0002
$1s^0 2s^1 2p^6$	–	0.0203	0.0090	–	0.0063	0.0018	–	0.0027	0.0006
$1s^0 2s^2 2p^5$	–	0.0410	0.0076	–	0.0128	0.0016	–	0.0054	0.0005
$1s^1 2s^0 2p^6$	0.3154	–	0.0080	0.0933	–	0.0016	0.0387	–	0.0005
$1s^1 2s^1 2p^5$	0.3112	0.0188	0.0068	0.0921	0.0059	0.0014	0.0382	0.0025	0.0004
$1s^1 2s^2 2p^4$	0.3073	0.0377	0.0056	0.0909	0.0118	0.0011	0.0378	0.0050	0.0003
$1s^2 2s^0 2p^5$	0.5567	–	0.0046	0.1674	–	0.0009	0.0702	–	0.0003
$1s^2 2s^1 2p^4$	0.5510	0.0166	0.0038	0.1658	0.0052	0.0007	0.0696	0.0022	0.0002
$1s^2 2s^2 2p^3$	0.5455	0.0334	0.0029	0.1643	0.0105	0.0006	0.0690	0.0045	0.0002
$1s^0 2s^0 2p^6$	–	–	0.0097	–	–	0.0020	–	–	0.0006
$1s^0 2s^1 2p^5$	–	0.0221	0.0083	–	0.0068	0.0017	–	0.0029	0.0005
$1s^0 2s^2 2p^4$	–	0.0446	0.0068	–	0.0138	0.0014	–	0.0059	0.0004
$1s^1 2s^0 2p^5$	0.3157	–	0.0075	0.0931	–	0.0015	0.0385	–	0.0005
$1s^1 2s^1 2p^4$	0.3109	0.0204	0.0061	0.0917	0.0063	0.0013	0.0380	0.0027	0.0004
$1s^1 2s^2 2p^3$	0.3064	0.0411	0.0047	0.0904	0.0127	0.0010	0.0375	0.0054	0.0003
$1s^2 2s^0 2p^4$	0.5571	–	0.0042	0.1670	–	0.0009	0.0698	–	0.0003
$1s^2 2s^1 2p^3$	0.5511	0.0182	0.0032	0.1653	0.0057	0.0007	0.0692	0.0024	0.0002
$1s^2 2s^2 2p^2$	0.5445	0.0367	0.0022	0.1635	0.0114	0.0004	0.0686	0.0049	0.0001
$1s^0 2s^0 2p^5$	–	–	0.0089	–	–	0.0019	–	–	0.0006
$1s^0 2s^1 2p^4$	–	0.0240	0.0073	–	0.0074	0.0015	–	0.0031	0.0005
$1s^0 2s^2 2p^3$	–	0.0487	0.0056	–	0.0150	0.0012	–	0.0063	0.0004
$1s^1 2s^0 2p^4$	0.3154	–	0.0067	0.0930	–	0.0014	0.0383	–	0.0004
$1s^1 2s^1 2p^3$	0.3101	0.0223	0.0052	0.0914	0.0069	0.0011	0.0377	0.0029	0.0003
$1s^1 2s^2 2p^2$	0.3049	0.0450	0.0035	0.0899	0.0139	0.0007	0.0372	0.0059	0.0002
$1s^2 2s^0 2p^3$	0.5571	–	0.0036	0.1667	–	0.0007	0.0695	–	0.0002
$1s^0 2s^1 2p^2$	0.5499	0.0201	0.0024	0.1648	0.0062	0.0005	0.0688	0.0026	0.0002
$1s^2 2s^2 2p^1$	0.5422	0.0407	0.0013	0.1628	0.0125	0.0003	0.0681	0.0053	0.0001
$1s^0 2s^0 2p^4$	–	–	0.0080	–	–	0.0017	–	–	0.0005
$1s^0 2s^1 2p^3$	–	0.0263	0.0062	–	0.0080	0.0013	–	0.0034	0.0004
$1s^0 2s^2 2p^2$	–	0.0532	0.0042	–	0.0162	0.0009	–	0.0069	0.0003
$1s^1 2s^0 2p^3$	0.3144	–	0.0057	0.0928	–	0.0012	0.0383	–	0.0004
$1s^1 2s^1 2p^2$	0.3083	0.0245	0.0039	0.0910	0.0075	0.0008	0.0376	0.0032	0.0002
$1s^1 2s^2 2p^1$	0.3020	0.0494	0.0020	0.0893	0.0151	0.0004	0.0370	0.0064	0.0001
$1s^2 2s^0 2p^2$	0.5556	–	0.0027	0.1665	–	0.0006	0.0695	–	0.0002
$1s^2 2s^1 2p^1$	0.5472	0.0223	0.0014	0.1643	0.0068	0.0003	0.0687	0.0029	0.0001
$1s^2 2s^2 2p^0$	0.5378	0.0453	–	0.1619	0.0138	–	0.0679	0.0059	–
$1s^0 2s^0 2p^3$	–	–	0.0066	–	–	0.0014	–	–	0.0004
$1s^0 2s^1 2p^2$	–	0.0285	0.0045	–	0.0087	0.0009	–	0.0037	0.0003
$1s^0 2s^2 2p^1$	–	0.0578	0.0023	–	0.0177	0.0005	–	0.0075	0.0002
$1s^1 2s^0 2p^2$	0.3125	–	0.0042	0.0925	–	0.0009	0.0382	–	0.0003
$1s^1 2s^1 2p^1$	0.3053	0.0268	0.0022	0.0905	0.0082	0.0004	0.0374	0.0035	0.0001
$1s^1 2s^2 2p^0$	0.2966	0.0543	–	0.0883	0.0166	–	0.0367	0.0070	–
$1s^2 2s^0 2p^1$	0.5528	–	0.0015	0.1662	–	0.0003	0.0694	–	0.0001
$1s^2 2s^1 2p^0$	0.5413	0.0247	–	0.1633	0.0075	–	0.0685	0.0032	–
$1s^0 2s^0 2p^2$	–	–	0.0048	–	–	0.0010	–	–	0.0003
$1s^0 2s^1 2p^1$	–	0.0308	0.0025	–	0.0095	0.0005	–	0.0040	0.0002
$1s^0 2s^2 2p^0$	–	0.0619	–	–	0.0190	–	–	0.0080	–
$1s^1 2s^0 2p^1$	0.3097	–	0.0023	0.0920	–	0.0005	0.0380	–	0.0002
$1s^1 2s^1 2p^0$	0.2991	0.0294	–	0.0893	0.0090	–	0.0371	0.0038	–
$1s^2 2s^0 2p^0$	0.5471	–	–	0.1653	–	–	0.0690	–	–
$1s^0 2s^0 2p^1$	–	–	0.0027	–	–	0.0006	–	–	0.0002
$1s^0 2s^1 2p^0$	–	0.0328	–	–	0.0102	–	–	0.0043	–
$1s^1 2s^0 2p^0$	0.3036	–	–	0.0908	–	–	0.0377	–	–

Table 2. The minimum and maximum of decay rates of neon.

Decay rate/s^{-1}	Minimum	Maximum
R_a	2.6×10^{13}	0.9×10^{15}
R_f	3.0×10^{8}	2.3×10^{13}

Table 3. The minimum and maximum of the photoionization cross section σ_p of neon at different photon energies.

Photon energy E/keV	σ_p/cm^2	
	Minimum	Maximum
2	1.7×10^{-22}	4.0×10^{-20}
4	1.3×10^{-23}	0.6×10^{-20}
6	3.0×10^{-24}	1.7×10^{-21}
8	0.8×10^{-24}	0.7×10^{-21}

3. Results and discussion

3.1. Single-hollow atom population

By solving these coupled rate equations under the related parameters mentioned previously, we obtain the evolution of population $n_\alpha(t)$ for all configurations of the neon atom and its ions. The application of hollow atoms is very important; for example, the fluorescence decay of hollow atoms makes it possible to pump new atomic x-ray lasers with ultrashort pulse duration, extreme spectral brightness, and full temporal coherence.[33,34] Here, we only show $n_\alpha(t)$ of $1s^12s^22p^6$, expressed as $n_{126}(t)$, for different laser parameters, see Fig. 1. Figure 1(a) shows $n_{126}(t)$ for different W and E at $N_p = 10^{10}$, and for $N_p = 10^{11}$ as shown in Fig. 1(b). We find that $n_{126}(t)$ takes more time to reach its maximum, and the maximum decreases when varying E, N_p, and W, separately. First, photoionization cross-sections σ_p become smaller with increasing E. Second, the photon flux $J(t)$ becomes smaller with decreasing N_p. In both cases, the decrease of photoionization rates reduces the number of photoionized neon atoms. Third, the increase of W causes the rise of $J(t)$ to slow down, as shown in Fig. 2. This leads to a slower increase in photoionization rates and further reduces the number of photoionized neon atoms. Here, $1s^12s^22p^6$ configuration is an excited state and then Auger decay, fluorescence decay or further photoionization will occur, and these processes lead quickly to reduce $n_{126}(t)$. However, we observe that $n_{126}(t)$ does not decrease to 0 during the whole pulse for some parameters from Fig. 1.

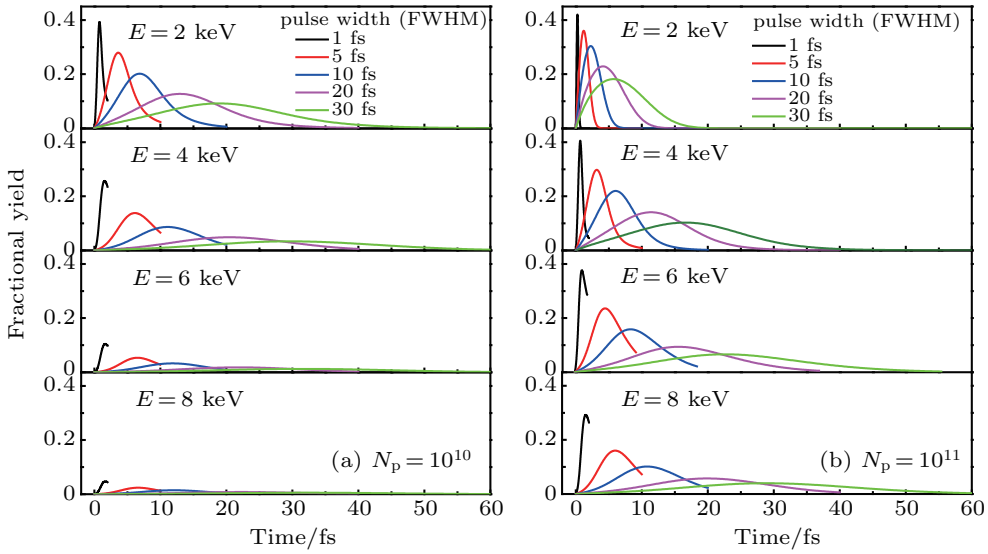


Fig. 1. The population evolution of $1s^12s^22p^6$ for different W (1 fs, 5 fs, 10 fs, 20 fs, 30 fs) and E (2 keV, 4 keV, 6 keV, 8 keV) at different N_p: (a) $N_p = 10^{10}$, (b)$N_p = 10^{11}$.

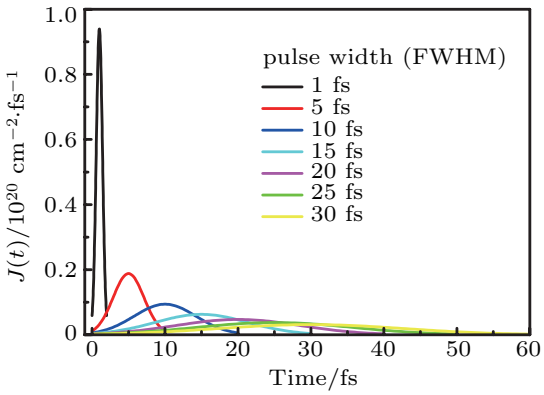


Fig. 2. The x-ray temporal pulse profile for different W at $N_p = 10^{10}$.

Therefore, by controlling these parameters, we can make $1s^12s^22p^6$ configuration retains its core vacancy during the pulse and further radiation damage is suppressed. If the next main process for $1s^12s^22p^6$ configuration is Auger decay and the pulse width is shorter than its Auger lifetime (≈ 2.7 fs), it can retain its core vacancy during the pulse. For example, when $E = 8$ keV, $W = 1$ fs, and $N_p = 10^{10}$, the maximum of R_a, R_f, and σ_p of $1s^12s^22p^6$ are 2.4134×10^{14} s^{-1}, 0.5613×10^{13} s^{-1}, 3.800×10^{-22} cm^2, and the corresponding orders of magnitude are 10^{14} s^{-1}, 10^{13} s^{-1}, and 10^{-22} cm^2. Under this laser parameter, the minimum and maximum of R_p changing with time are 2.0×10^{12} s^{-1} and 3.5×10^{13} s^{-1},

and the corresponding the order of magnitude is 10^{12} s^{-1} $\sim$ 10^{13} s^{-1}. So, the next main process for $1s^1 2s^2 2p^6$ is Auger decay, it retains core vacancy during the pulse, as shown in Fig. 1(a).

3.2. Charge-states

The population evolution $n_i(t)$ of different charge-states is obtained by summing over the population evolution of each configuration belongings to the respective ion.

$$n_i(t) = \sum_{\alpha}^{\text{config}} n_\alpha(t), \tag{13}$$

where $n_i(t)$ is the population evolution of Ne^{i+}. However, the measured populations in the experiment are time-independent average results. They can be obtained by the time-average,

$$n_i = \frac{\int_0^{t_0} n_i(t)\,\mathrm{d}t}{t_0}, \tag{14}$$

where t_0 is the total time of the pulse acts on atoms and n_i is the time-independent population of a certain charge-state. Here we use n_0 for the population of the neutral neon atom, n_i for the population of Ne^{i+}, with $i = 1, 2, 3, \ldots, 10$. Using laser parameters in Ref. [2], we simulate the experimental results by the method mentioned previously, and compare the calculated results with the experimental data and other theoretical simulation, as shown in Fig. 3. We find that our simulation results are in fair agreement with experiment. But both our results and previous theoretical results have a slight difference with the experimental results because we only consider three main processes in the simulation process. When neon is irradiated by XFEL, other complex processes arise.

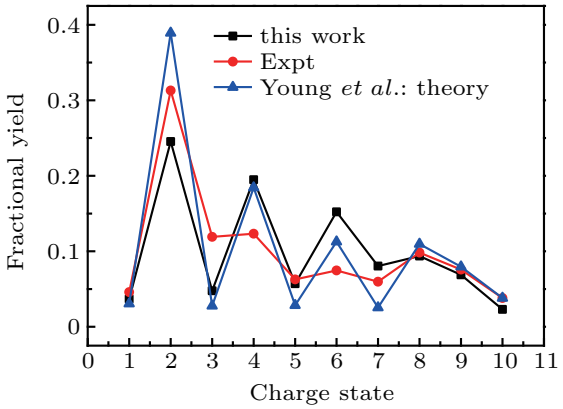


Fig. 3. Charge-states populations of neon irradiated with x-ray pulses compared with experimental data[2] and other theoretical result.[2]

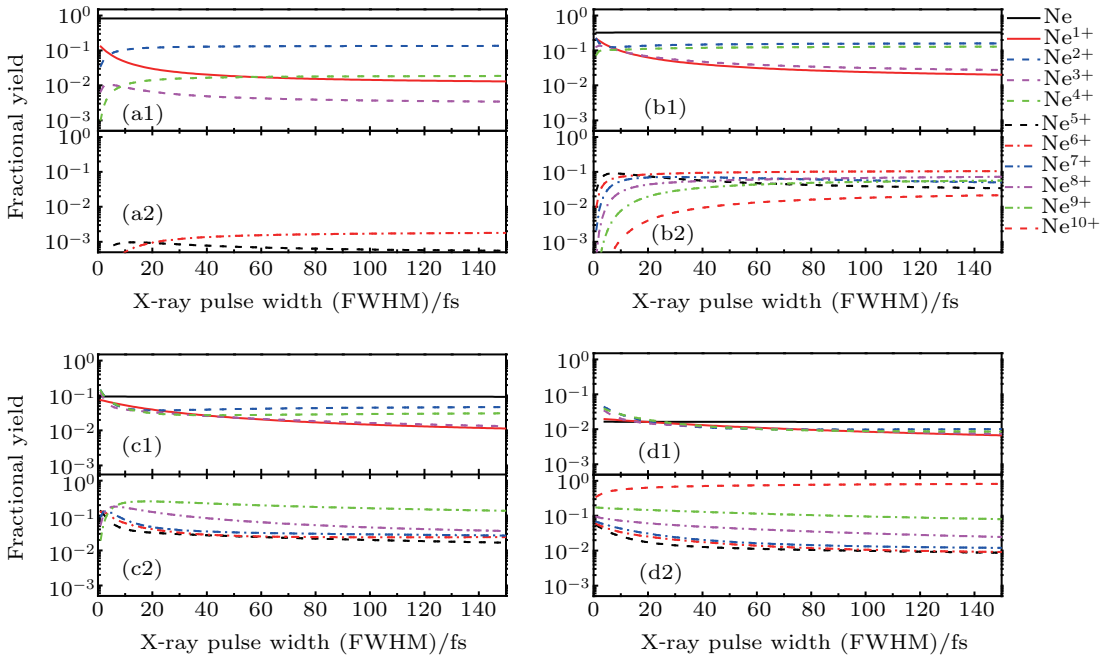


Fig. 4. Populations n_i for Ne $\sim$ Ne^{10+} as a function of the pulse width W for $E = 2$ keV with different N_p: (a) $N_p = 10^9$, (b) $N_p = 10^{10}$, (c) $N_p = 10^{11}$, and (d) $N_p = 10^{12}$.

Figure 4 shows the variations of $n_0, n_1, \ldots, n_{10}$ with pulse width W at $E = 2$ keV for different N_p. To make the figure clearer, we divide $n_0, n_1, \ldots, n_{10}$ under the same laser parameters into two groups, such as (a1), (a2) in Fig. 4. Figure 4(a1) shows n_0, n_1, n_2, n_3, and n_4. And n_5 to n_{10} are shown in Fig. 4(a2), but figure 4(a2) only shows the n_5 and n_6, because n_7, n_8, n_9, and n_{10} are negligible. So, the population n_i of an arbitrary charge-state under a given parameter can be obtained from Fig. 4. Figure 4 shows that these n_i have a major trend: every charge-state n_i has a certain change when W is shorter than 10 fs at the same N_p. Certain charge-states n_i decrease rapidly, while others rise. The variations of n_i for different N_p are not completely uniform. For example, when W is shorter than 10 fs, n_4 increases rapidly with pulse width for $N_p = 10^9$, its growth rate slows for $N_p = 10^{10}$, but decreases for $N_p = 10^{11}$, 10^{12}. When W is larger than 10 fs, there is a ten-

dency for the variations to slow down, and then n_i remain relatively constant with increasing W. This happens because the variation of the x-ray temporal pulse profile becomes smaller with the increase of W when N_p is fixed, as shown in Fig. 2. With an increase of N_p, the population n_0 decreases gradually, and n_i of low-charge neon ions increase first and then decrease. These lead to the increase of high-charge n_i. The population n_0 dominates at $N_p = 10^9$ or 10^{10}, but n_{10} takes over at $N_p = 10^{11}$ or 10^{12}. At $N_p = 10^9$, n_5 and n_6 are small, while $n_7 \sim n_{10}$ are negligibly small and not shown in Fig. 4(a). So, even if the pulse width is very large, the neon can only be ionized up to Ne^{5+} and Ne^{6+}. Neon is more likely to be ionized to higher charge-states with increasing N_p.

Figure 5 shows the variation of n_i with W for different E at $N_p = 10^9$. The population n_i of the same charge-state decreases with increasing E. The highest charge-state is Ne^{4+} at $E = 4$ keV, and the highest charge-state is Ne^{2+} at $E = 6$ keV and 8 keV.

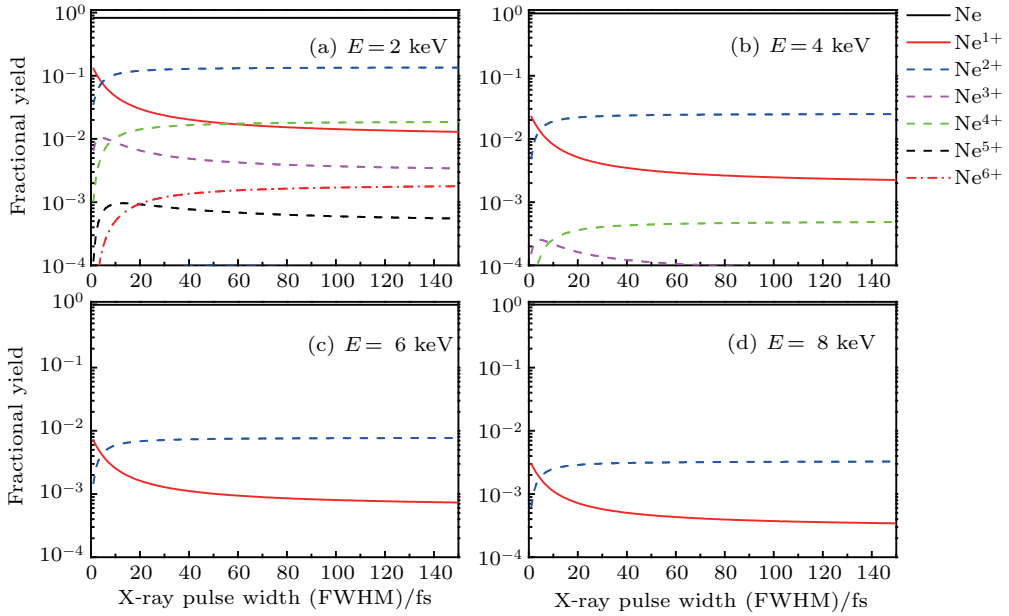


Fig. 5. The variation of populations n_i with the pulse width W for $N_p = 10^9$ at different E: (a) 2 keV, (b) 4 keV, (c) 6 keV, and (d) 8 keV.

3.3. Average charge

To make it easier to understand the results of Figs. 4 and 5, we calculate the average charge of ions under different conditions. The average charge $\overline{Z}$ is given by

$$\overline{Z} = \sum_{i}^{\text{all ions}} Z_i n_i, \tag{15}$$

where Z_i is the charge of the i-th ion. Figure 6 shows the average charge $\overline{Z}$ as a function of W for different N_p and E. We find that the average charge $\overline{Z}$ increases with increasing N_p while keeping E and W constant. As shown in Fig. 6(a), the minimum of $\overline{Z}$ is about 0.2 for $N_p = 10^9$, and gradually approaches 0.4 with increasing W. But the minimum of $\overline{Z}$ is about 7 at $N_p = 10^{12}$, and gradually approaches 10 with increasing W. This suggests that, even if the pulse width is narrow, seven electrons or more may be stripped, and this results in serious radiation damage. Furthermore, the average charge $\overline{Z}$ decreases with increasing E while keeping N_p constant, because the photoionization cross sections become smaller with increasing E, as shown in Table 1. So a higher photon energy induces less electronic damage. And the average charge $\overline{Z}$ begins to decrease for pulse width shorter than 10 fs but remains basically unchanged for the pulse width longer than 10 fs. This corresponds to the situation shown in Figs. 4 and 5.

To make this point clear, we have obtained the most prominent ionization pathways with different laser parameters. From the calculated photoionization cross sections, Auger decay rates, and fluorescence decay rates, we know that ionization pathways are much more complex. If photoionization rates, Auger decay rates, and fluorescence decay rates are time-independent constants, the most prominent ionization pathway is obtained by comparing these photoionization and decay rates.[20] But the photoionization rate R_p is a function of time in this paper, and we obtain the most prominent ionization pathway by the most important product. Take the first step and the second step of the most prominent ionization pathway at $E = 2$ keV, $N_p = 10^{10}$, and $W = 1$ fs as an example. The next possible ionization processes for $1s^2 2s^2 2p^6$ are shown in Fig. 7(a), which can be photoionized as product configurations $1s^1 2s^2 2p^6$, $1s^2 2s^1 2p^6$, $1s^2 2s^2 2p^5$. These product configurations become other configurations through various ionization processes, and the yields of product configurations are not easy to determine. If the source of the product configuration is set to be $1s^2 2s^2 2p^6$ only, and rate coefficients of the product configuration ionized to other configurations are set to 0, the yields of product configurations can be obtained, as shown in Fig. 8(a). It is found that the yield of $1s^1 2s^2 2p^6$ is much higher than that of other products, so $1s^1 2s^2 2p^6$ is the

most important product. Furthermore, $1s^12s^22p^6$ could be ionized to become product configurations $1s^02s^22p^6$, $1s^12s^12p^6$, $1s^12s^22p^5$, $1s^22s^22p^5$, $1s^22s^22p^4$, $1s^22s^12p^5$, $1s^22s^02p^6$, see Fig. 7(b). And the yields of these product configurations are shown in Fig. 8(b), the yield of $1s^02s^22p^6$ is much higher than that of other products, so $1s^02s^22p^6$ is the most important product. Thus, the most prominent ionization process of $1s^12s^22p^6$ is photoionization of the inner-shell electron. So, the first step and the second step of the most prominent ionization pathway are photoionization processes at $E = 2$ keV, $N_p = 10^{10}$, and $W = 1$ fs. The most prominent ionization process of each step can be determined by the above method.

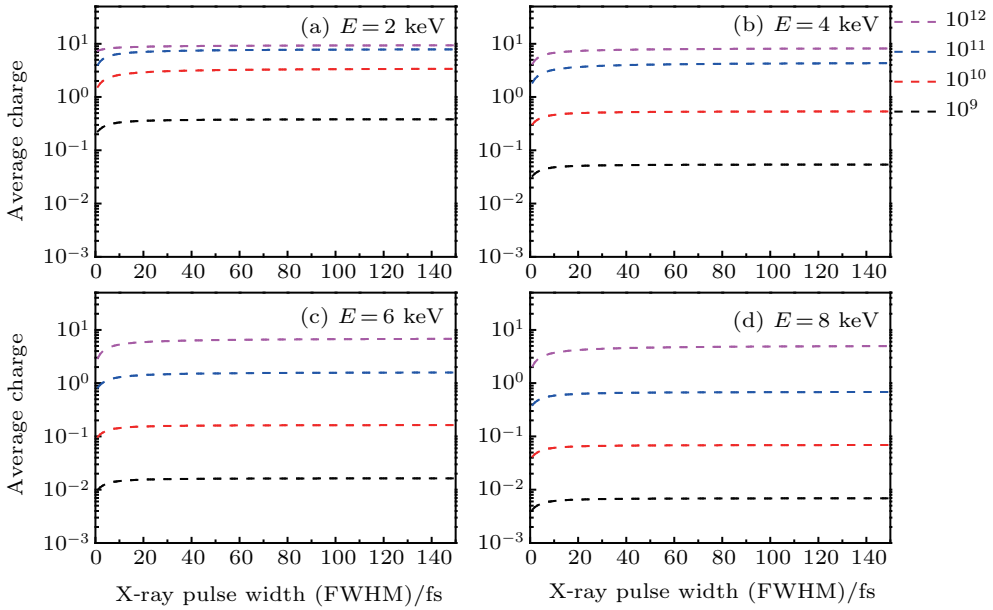


Fig. 6. Variations of the average charge $\overline{Z}$ with pulse width W for different N_p and different E: (a) 2 keV, (b) 4 keV, (c) 6 keV, and (d) 8 keV.

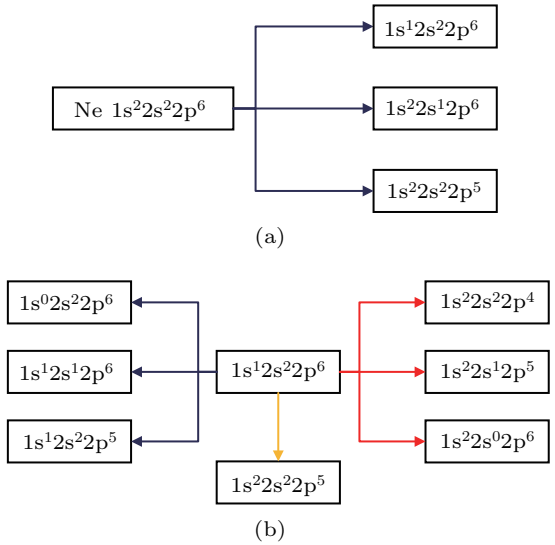


Fig. 7. (a) Ionization processes of $1s^22s^22p^6$; (b) Ionization processes of $1s^12s^22p^6$. The blue arrow represents photoionization, the red arrow represents Auger decay, the yellow arrow represents fluorescence decay.

Figure 9 shows the most prominent ionization pathways at 2 keV for W being shorter than 10 fs and different N_p. It has been found that the most prominent ionization pathways of Ne are different with different laser parameters, which is mainly due to the change of photoionization rates. Photoionization rates of the configuration increase while its Auger decay rates and fluorescence decay rates remain unchanged with increasing of $J(t)$ or decreasing E. Therefore, decay processes are gradually inhibited, and continuous photoionization processes are more likely to occur. Figure 9(a) shows that the most prominent pathway to produce Ne^{6+} through absorption of four photons is PPAPAP for $W = 1$ fs and Ne^{8+} is PPAPAPAP for $W = 2$ fs $\sim$ 4 fs. Although the most prominent pathway is different for $W = 5$ fs $\sim$ 10 fs, the neutral neon atom can be ionized to a bare nucleus by absorbing six photons. That is, the neutral atom and low charge-states are gradually transformed into higher charge-states with increasing pulse width. Therefore, in Fig. 6(a), the decrease of the average charge $\overline{Z}$ before 10 fs for $N_p = 10^{10}$ can be understood as follows. The highest charge-state possible becomes low

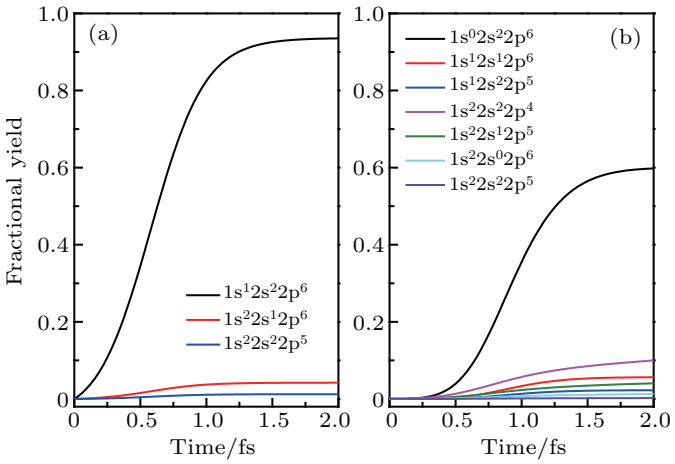


Fig. 8. The yields of product configurations of $1s^22s^22p^6$ and $1s^12s^22p^6$ at $N_p = 10^{10}$, $W = 1$ fs, and $E = 2$ keV. (a) $1s^22s^22p^6$; (b) $1s^12s^22p^6$.

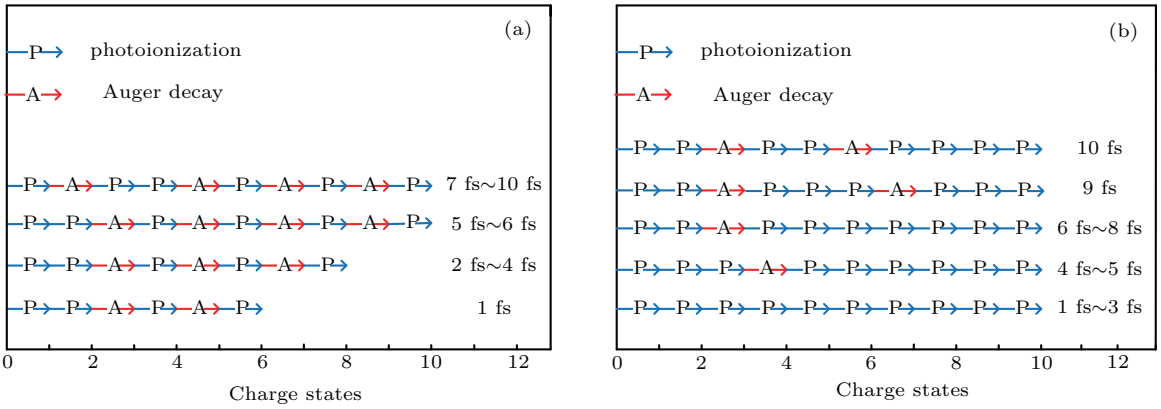


Fig. 9. The most prominent ionization pathways for pulse width shorter than 10 fs at 2 keV for different N_p: (a) $N_p = 10^{10}$ and (b) $N_p = 10^{12}$. P represents photoionization and A represents Auger decay.

with decreasing pulse width because the pulse is too short to generate a higher charge-state. And the population n_i of the highest charge-state decreases with decreasing pulse width, as evident in Fig. 4(b). Figure 9(b) shows that the neon atom can be ionized to a bare nucleus for $N_p = 10^{12}$ by the most prominent pathways with different W. In other words, the average charge $\overline{Z}$ is very high starting from $W = 1$ fs. The reason of the average charge $\overline{Z}$ has a downward trend ahead of 10 fs for $N_p = 10^{12}$ is that there are other non-primary pathways besides the decrease in the population n_i of the highest charge-state. Other pathways have characteristics similar to that in Fig. 9(a), in which the neutral atom and low charge-states are gradually transformed into higher charge-states with increasing pulse width.

4. Conclusion

The interaction between the neon atom and x-ray free-electron lasers is systematically studied by varying the photon energy from 2 keV to 8 keV, the number of incident photon from 10^9 to 10^{12} and the pulse width from 1 fs to 150 fs with a Gaussian profile. By solving the rate equations associated with these parameters, we obtain the evolution of configurations as functions of these three laser pulse parameters. At $N_p = 10^{10}$ and 10^{11}, the population evolution of $1s^1 2s^2 2p^6$ configuration is given as an example to show the dynamics at different pulse widths and photon energies. Further, by averaging over time, we determined all charge-state populations from the neutral atom to the bare ion as a function of these three laser pulse parameters. The variations of charge-state populations show certain pattern when the pulse width is shorter than 10 fs, *i.e.*, certain charge-state populations decrease rapidly, while others rise. For a pulse width larger than 10 fs, the tendency of variations slows down and then remains relatively constant with increasing pulse width, see Subsection 3.1 for further details. Subsequently, the variation of average charge with three parameters is obtained. The average charge decreases for pulse width shorter than 10 fs but remains basically unchanged for a pulse width longer than 10 fs. The reason for the decline is that the ionized highest charge-state decreases with decreasing pulse width; that is, the pulse is too short to generate higher charge-states and the population of the highest charge-state also decreases with decreasing pulse width.

References

[1] Pellegrini C, Marinelli A and Reiche S 2016 *Rev. Mod. Phys.* **88** 015006
[2] Young L, Kanter E P, Krässig B *et al.* 2010 *Nature* **466** 56
[3] Emma P, Akre R, Arthur J *et al.* 2010 *Nat. Photon.* **4** 641
[4] Ishikawa T, Aoyagi H, Asaka T *et al.* 2012 *Nat. Photon.* **6** 540
[5] Kang H S, Min C K, Heo H *et al.* 2017, *Nat. Photon.* **11** 708
[6] Tschentscher T, Bressler C, Grünert J, Madsen A, Mancuso A P, Meyer M, Scherz A, Sinn H and Zastrau U 2017 *Applied Science-Based* **7** 592
[7] Milne C J, Schietinger T, Aiba M *et al.* 2017 *Applied Sciences-Basel* **7** 720
[8] Milne C J, Beaud P, Deng Y P, Erny C, Follath R, Flechsig U, Hauri P C, Ingold G, Juranic P, Knopp G, Lemke H, Pedrini B, Radi P, and Patthey L 2017 *Chimia* **71** 299
[9] Galayda J N 2014 *in Proceedings of the 2014 International Particle Accelerator Conference*, Dresden, Germany, p. 935
[10] Son S K, Young L and Santra R 2011 *Phys. Rev. A* **83** 033402
[11] Feldhaus J, Arthur J and Hastings J B 2005 *Phys. B: At. Mol. Opt. Phys.* **38** S799
[12] Bostedt C, Boutet S, Fritz D M, Huang Z R, Lee H J, Lemke H T, Robert A, Schlotter W F, Turner J J and Williams G J 2016 *Rev. Mod. Phys.* **88** 015007
[13] Ho P J, Bostedt C, Schorb S and Young L 2014 *Phys. Rev. Lett.* **113** 253001
[14] Hoener M, Fang L, Kornilov O *et al.* 2010 *Phys. Rev. Lett.* **104** 253002
[15] Mankowsky R, Subedi A, Först M, Mariager S O, Chollet M, Lemke H T, Robinson J S, Glownia J M, Minitti M P, Frano A, Fechner M, Spaldin N A, Loew T, Keimer B, Georges A and Cavalleri A 2014 *Nature* **516** 71
[16] Vinko S M, Ciricosta O, Cho B I *et al.* 2012 *Nature* **482** 59
[17] Zhang W K, Alonso-Mori R, Bergmann U *et al.* 2014 *Nature* **509** 345
[18] Zhou Q J, Lai Y, Bacaj T, Zhao M L, Lyubimov A Y, Uervirojnangkoorn M, Zeldin O B, Brewster A S, Sauter N K, Cohen A E, Soltis S M, Alonso-Mori R, Chollet M, Lemke H T, Pfuetzner R A, Choi U B, Weis W I, Diao J J, Südhof T C and Brunger A T 2015 *Nature* **525** 62
[19] Fan J D and Jiang H D 2012 *Acta Phys. Sin.* **61** 218702 (in Chinese)
[20] Lei F and Gang J 2017 *Acta Phys. Sin.* **66** 153201 (in Chinese)

[21] Yoneda H, Inubushi Y, Yabashi M, Katayama T, Ishikawa T, Ohashi H, Yumoto H, Yamauchi K, Mimura H and Kitamura H 2014 *Nat. Commun.* **5** 5080

[22] Nagler B, Zastrau U, Fäustlin R R *et al.* 2009 *Nat. Phys.* **5** 693

[23] Moribayashi K, Sasaki A and Tajima T 1998 *Phys. Rev. A* **58** 2007

[24] Rohringer N and Santra R 2007 *Phys. Rev. A.* **76** 033416

[25] Gao C, Zeng J L and Yuan J M 2015 *High Energy Density Physics* **14** 52

[26] Gao C, Zeng J L and Yuan J M 2016 *J. Phys. B: At. Mol. Opt. Phys.* **49** 044001

[27] Ciricosta O, Chung H K, Lee R W and Wark J S 2011 *High Energy Density Physics* **7** 111

[28] Xiang W J, Gao C, Fu Y S, Zeng J L and Yuan J M 2012 *Phys. Rev. A.* **86** 061401

[29] Gu M F 2008 *Can. J. Phys.* **86** 675

[30] Tschentscher T, Altarelli M, Brinkmann R, Delissen T, Schwarz A S and Witte K 2006 *Synchrotron Radiation News* **19** 13

[31] Lei F 2017 "Hollow atoms formation and x-ray transparency of Ne in 2000 eV XFEL research basing on ionization route," MS Dissertation (Chengdu: Sichuan University) (in Chinese)

[32] Bethe H A and Salpeter E E 1977 *Quantum Mechanics of One- and Two-Electron Atoms* (New York: Plenum Publishing Corporation) p. 300

[33] Yoneda H, Inubushi Y, Nagamine K, Michine Y, Ohashi H, Yumoto H, Yamauchi K, Mimura H, Kitamura H, Katayama T, Ishikawa T and Yabashi M 2015 *Nature* **524** 446

[34] Rohringer N, Ryan D, London R A, Purvis M, Albert F, Dunn J, Bozek J D, Bostedt C, Graf A, Hill R, Hau-Riege S P and Rocca J J 2012 *Nature* **481** 488